

Intrinsic Lithiophilicity of Li–Garnet Electrolytes Enabling High-Rate Lithium Cycling

Hongpeng Zheng, Shaoping Wu, Ran Tian, Zhenming Xu, Hong Zhu, Huanan Duan,* and Hezhou Liu

Solid-state lithium batteries are widely considered as next-generation lithium-ion battery technology due to the potential advantages in safety and performance. Among the various solid electrolyte materials, Li–garnet electrolytes are promising due to their high ionic conductivity and good chemical and electrochemical stabilities. However, the high electrode/electrolyte interfacial impedance is one of the major challenges. Moreover, short circuiting caused by lithium dendrite formation is reported when using Li–garnet electrolytes. Here, it is demonstrated that Li–garnet electrolytes wet well with lithium metal by removing the intrinsic impurity layer on the surface of the lithium metal. The Li/garnet interfacial impedance is determined to be $6.95 \Omega \text{ cm}^2$ at room temperature. Lithium symmetric cells based on the Li–garnet electrolytes are cycled at room temperature for 950 h and current density as high as 13.3 mA cm^{-2} without showing signs of short circuiting. Experimental and computational results reveal that it is the surface oxide layer on the lithium metal together with the garnet surface that majorly determines the Li/garnet interfacial property. These findings suggest that removing the superficial impurity layer on the lithium metal can enhance the wettability, which may impact the manufacturing process of future high energy density garnet-based solid-state lithium batteries.

1. Introduction

As the applications of Li-ion batteries have grown from consumer electronics to electric vehicles and stationary power systems, the limitations of this technology have become more apparent. Specifically, the conflict between the continuously increasing energy density and the inherent safety concerns in conventional Li-ion battery technology needs to be addressed more urgently than ever. Many research endeavors have been


dedicated to improving these properties (i.e., energy density and safety), but the cost and energy density of Li-ion technology are reaching a plateau and a revolutionary transformation is needed.^[1]

Now, it is widely accepted that solid-state batteries represent the next-generation of battery technology.^[2] Solid-state electrolytes (SSEs), such as garnet-type $\text{Li}_7\text{La}_3\text{Zr}_2\text{O}_{12}$ (LLZO), are usually nonflammable and ultimately safe.^[3] Among the various SSE materials, lithium–garnets have attracted much attention due to their good chemical/electrochemical stability with electrode materials, close-to-unity transference number, and high room-temperature ionic conductivity (10^{-3} – $10^{-4} \text{ S cm}^{-1}$), although, a typical liquid electrolyte has ionic conductivity up to $10^{-2} \text{ S cm}^{-1}$ and a transference number ≈ 0.3 .^[3a,4] However, the high interfacial impedance between SSE and electrodes have severely hindered the full-cell development. The Li/garnet interface is particularly significant for the following reasons:^[3a,4b,5] 1) garnet since its discovery has been regarded as stable toward Li, which eventually becomes one of its main advantages; 2) Li/garnet interface with low impedance and relative stability may enable battery systems based on new chemistry such as Li–air and Li–S batteries.

One of the major challenges facing Li/LLZO interfaces is the sluggish Li-ion transport across the interface signified by a large interfacial resistance.^[6] This is partially related to the poor physical contact for the solid-solid Li/LLZO interface.^[7] As a result, early attempts to improve the Li/LLZO interfacial properties consist of heating the Li anode and maintaining high pressure between Li and LLZO to improve the interfacial contact.^[8] More recently, significant advances have been achieved in developing a desirable Li/LLZO interface by modifying the LLZO. Various strategies have been proposed such as densifying LLZO pellets by hot isostatic pressing (HIP),^[9] adding an interlayer (Al_2O_3 , Si, Au, C) on the LLZO surface that can react or form an alloy with Li during electrochemical cycling,^[8a,10] chemically or mechanically treating the LLZO surface to eliminate the effect of the superficial Li_2CO_3 layer that may form during sample processing or storage,^[4c,11] and increasing the contact area by making the LLZO surface porous.^[12] With all these efforts, the Li/LLZO interfacial resistance has been reduced to $\approx 1 \Omega \text{ cm}^2$.^[10a]

H. Zheng, S. Wu, R. Tian, Prof. H. Duan, Prof. H. Liu
State Key Laboratory of Metal Matrix Composites
School of Materials Science and Engineering
Shanghai Jiao Tong University
Shanghai 200240, P. R. China
E-mail: hd1@sjtu.edu.cn

Z. Xu, Prof. H. Zhu
University of Michigan–Shanghai Jiao Tong University Joint Institute
Shanghai Jiao Tong University
Shanghai 200240, P. R. China

 The ORCID identification number(s) for the author(s) of this article can be found under <https://doi.org/10.1002/adfm.201906189>.

DOI: 10.1002/adfm.201906189

Another challenge is that the ability to suppress Li-dendrite formation and propagation during cycling. In this sense, critical current density (CCD), at which the cell will be shorted, is important to index the Li-ion transport capability across the Li/SSE interface and the ability to suppress the Li dendrites because the higher the cycling current densities, the greater the possibility of dendrite formation due to inhomogeneous dissolution and deposition of metallic Li at the Li/garnet interfaces.^[1g,13] Tremendous efforts have been dedicated to improving the Li/garnet interfaces and increasing the CCD. For example, HIP has been used to make well-densified garnet pellets because lithium dendrites were found to possibly form through grain boundaries and interconnected pores in the ill-densified pellets.^[14] Indeed, a current density of 0.5 mA cm⁻² was obtained without the occurrence of dendrite-related short circuiting.^[9] This means that a well-densified garnet pellet is fundamental to attaining high CCD. Subsequently, grain boundaries of the garnet were engineered through second-phase doping (i.e., Li₃PO₄, LiCl) to suppress the Li-dendrite formation by taking advantage of the self-limited interaction between the dopant and the freshly deposited Li, but the current density did not exceed 0.1 mA cm⁻².^[15] With the understanding of the surface chemistry of garnet pellets, specifically, the correlation between the formation of Li₂CO₃ when keeping the pellets in moist environment and the Li/garnet interfacial impedance,^[16] various methods were trialed to reduce if not remove the surface Li₂CO₃ layer.^[4c,10d,11a,b,17] Evidently, the interfacial impedance was effectively reduced, but the CCD was merely 0.3 mA cm⁻².^[11b] An experimental progress was reported where ultrathin Al₂O₃ was found to significantly decrease the Li/garnet interfacial impedance from 1710 to 1 Ω cm², but the current density of the corresponding symmetric cells is 0.2 mA cm⁻².^[10a] Other surface modification approaches have been proposed and different interlayer materials such as Al, Sn, C, Si, MoS₂, have been trialed with similar purpose.^[6,8,10a,c,d,17,18] In spite of all these efforts, to the best of our knowledge, the highest reported CCD value of planar lithium–garnets is still less than 0.9 mA cm⁻² at room temperature.^[6] By contrast, the CCD of liquid electrolytes can reach 4–10 mA cm⁻² at room temperature.^[13] Meanwhile, none of these studies is dedicated to investigating the effect of Li metal.

Here, we demonstrate that the surface oxide layer on lithium metal together with the garnet surface determines the Li/garnet interfacial property. By removing the superficial impurity layer on the Li metal, Li/garnet electrolytes exhibit intrinsic lithiophilicity, enabling a critical current density as high as 13.3 mA cm⁻² at room temperature and a stable high-rate lithium cycling of the symmetric cells for hundreds of cycles. The effects of the surface oxide layer on Li metal and Li₂CO₃ on garnet surface are analyzed through various experimental techniques as well as first-principle calculations.

2. Results and Discussion

2.1. Li Metal–Li_{6.4}La₃Zr_{1.4}Ta_{0.6}O₁₂ (LLZT) Interface Property

The scanning electron microscopy (SEM) image (Figure S1, Supporting Information) of the LLZT pellets shows that the LLZT is well densified after sintering by a solid-state reaction

process at 1140 °C for 16 h. The relative density of the LLZT pellets is about 94% by measuring the mass and the volume of the pellets and normalized to the theoretical density of 5.10 g cm⁻³.^[19] The resulting LLZT pellets were 1 mm thick with a surface area of 1.13 cm². X-ray diffraction (XRD) patterns (Figure S2, Supporting Information) of the LLZT indicate that all peaks can be assigned to the cubic garnet phase (PDF #45-0109), implying that a fast Li-ion conducting cubic garnet phase is obtained. Ionic conductivity of the LLZT was evaluated by electrochemical impedance spectroscopy (EIS) with Ag electrodes at temperatures from 20 to 90 °C. As shown in Figure S3a (Supporting Information), the ionic conductivity at 20 °C is determined to be about 2 × 10⁻⁴ S cm⁻¹ by fitting, and the activation energy of the Li⁺ conduction within the LLZT is 0.29 eV, as determined in Figure S3b (Supporting Information). These conductivity and activation energy values are well within the previously reported range.^[4a]

The Li metal/LLZT interfacial resistance was examined by testing the symmetric Li/garnet/Li cells using EIS technique. Symmetric cells were assembled in an Ar-filled glovebox with two methods: 1) sandwiching LLZT pellets between two Li foils (designated as Li_s/LLZT/Li_s), heating the stacked cell up to 300 °C to improve the Li/LLZT contact, followed by cooling and making coin-cell under pressure of about 5 MPa; and 2) rubbing the LLZT pellets on molten Li till the Li wets the garnet surface (designated as Li_r/LLZT/Li_r, as shown in Video S1 in the Supporting Information), followed by cooling and coin-cell making. The cooled cells were then subjected to EIS measurements. As shown in Figure 1a, the Nyquist plots of the Li_r/LLZT/Li_r cells exhibit one semicircle in the high and medium frequency region followed by a tail at a low frequency. The garnet resistance can be determined from the distance between zero point and the high-frequency *x*-intercept of the semicircle; the semicircle at the high and medium frequencies arises from the charge transfer resistance (the interfacial resistance); the tail at low frequency may be attributed to the Li⁺ diffusion process, which is related to the contact between the lithium metal and garnet electrolyte.^[10d,18] By fitting with the equivalent circuit shown in the inset of Figure 1a, the ionic conductivity of the LLZT is determined to be 7.36 × 10⁻⁴ S cm⁻¹, which is significantly larger than the value determined by using Ag blocking electrodes (2 × 10⁻⁴ S cm⁻¹). It implies that the rub-coating technique provides a better metal/LLZT contact than the Ag paste. Furthermore, the interfacial area specific resistance (ASR) is determined by dividing the interfacial resistance by two and normalizing to the electrode surface area. The fitting results show that the interfacial ASR of the Li_r/LLZT/Li_r cells is 6.95 Ω cm² at 25 °C. The interfacial ASR decreases with increasing temperature, as shown in Figure 1b. Figure S4 (Supporting Information) compares the present interfacial ASR value with the ASR values reported in the literature.^[8a,10c,d,17,20] Evidently, the present work provides the lowest interfacial ASR for all the Li/garnet interfaces without any surface modification.

The cross-sectional SEM images of the Li/LLZT interfaces were collected to analyze the reason for this small interfacial ASR. As shown in Figure 1c–f, metallic Li is tightly bonded to LLZT and forms a continuous and intimate interfacial contact by rub coating molten Li, implying the intrinsic lithiophilicity of LLZT electrolyte. By contrast, stacking and mechanically

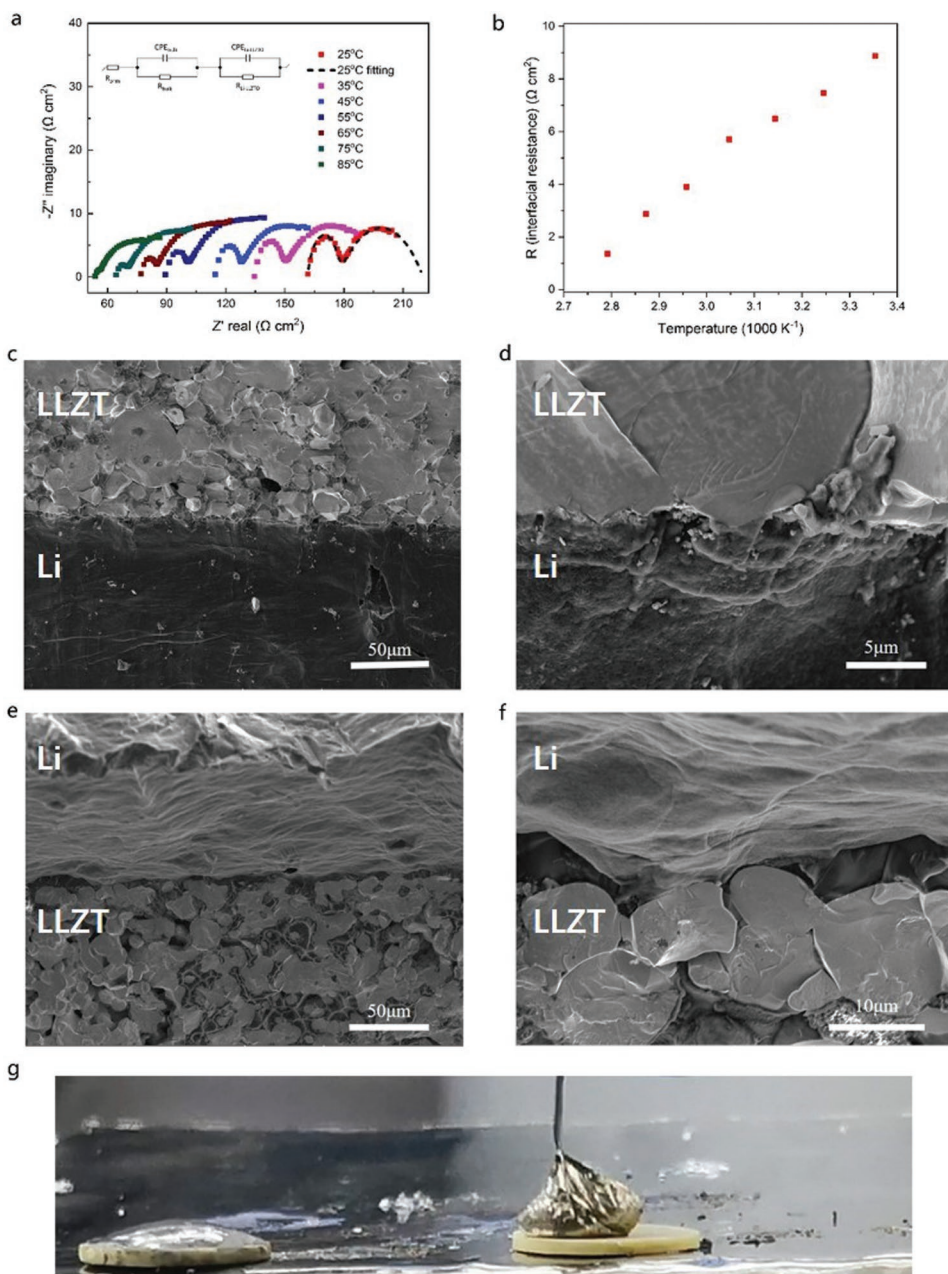


Figure 1. Characterization of the Li/LLZT interfaces. a) Nyquist plots of $\text{Li}_r/\text{LLZT}/\text{Li}_r$ symmetric cells at temperatures from 25 to 85 °C. Inset shows the equivalent circuit used for modeling the EIS data. b) Arrhenius plot of the interfacial resistance of Li_r/LLZT . c–f) SEM images of the LLZT/Li metal interface by two different adding methods, rubbing (c, d) and stacking (e, f). g) Images of the melted Li metal on top of the LLZT surface after rub coating and stacking.

pressing only offer poor interface contact, leading to a high interfacial ASR. This difference is observed in Figure 1g, where molten Li wetted LLZT properly and maintained good contact after rub coating. However, the other method where lithium was stacked and heated directly on LLZT pellet came off when attempts were made to remove the lithium foil intentionally. We speculate that there may be an impurity layer on the lithium surface that hinders the wetting between the stack-coated lithium and LLZT; whereas rub coating may break the impurity layer and expose the LLZT pellets to fresh molten lithium, so that LLZT could effectively wet molten lithium.

To evaluate the electrochemical stability and Li stripping and plating performance, cyclic voltammetry analysis of the Li_r/LLZT was performed at room temperature. As displayed in Figure S5 (Supporting Information), the cathodic and anodic peaks corresponding to the plating/stripping of the lithium metal are observed near 0 V. Moreover, no other decomposition current is observed in the scanned potential range up to 6 V, indicating that the garnet maintains stability during the Li stripping and plating. The critical current density and Li cycling behavior were characterized using a combination of DC cycling and EIS analysis to evaluate the Li-ion transport capability

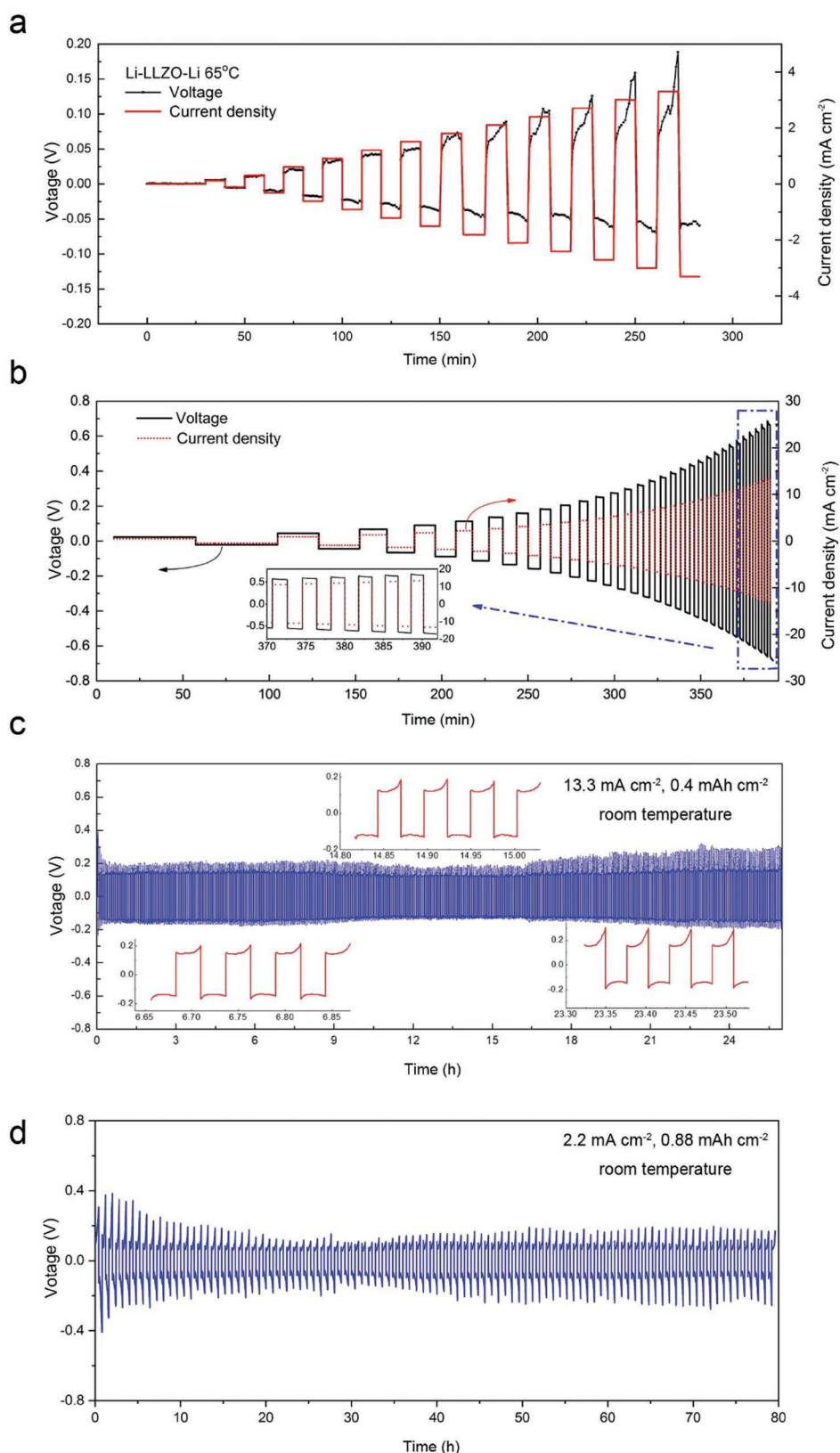


Figure 2. Electrochemical characterization of the Li/LLZO interfaces. a) Galvanostatic cycling of symmetric $\text{Li}_r/\text{LLZO}/\text{Li}_r$ cells at 65°C with fixed stripping/plating time of 10 min, stepping the current density from 0.01 to 3.3 mA cm^{-2} . b) Galvanostatic cycling of symmetric $\text{Li}_r/\text{LLZO}/\text{Li}_r$ cells at room temperature with fixed stripping/plating capacity of 0.36 mAh cm^{-2} , stepping the current density from 0.5 to 13.3 mA cm^{-2} . c,d) Galvanostatic cycling of $\text{Li}_r/\text{LLZO}/\text{Li}_r$ at various conditions: 13.3 mA cm^{-2} at 0.4 mAh cm^{-2} for 500 cycles (c), 2.2 mA cm^{-2} at 0.88 mAh cm^{-2} for 100 cycles (d).

across the Li_r/LLZT interface (Figure 2). The CCD is defined as the lowest current density at which cell shorting occurs due to Li dendrite penetration.^[8b,21] We first fixed the duration of Li plating and stripping to 10 min, and obtained a CCD of 3.3 mA cm^{-2} with a maximum capacity of 0.55 mAh cm^{-2} at 65°C (Figure 2a). Further current increase was prevented by the significant potential perturbation, which is associated with the formation and disappearance of voids at the Li/LLZT interface.^[22] The accumulation of voids and/or the formation of occluded voids during cycling will cause deterioration of the Li/LLZT contact, increasing polarization, and severe potential perturbation at high current densities.^[1g,23] As a result, we fixed the cycling capacity to 0.36 mAh cm^{-2} to limit the potential perturbation. A CCD of 13.3 mA cm^{-2} was achieved at room temperature (Figure 2b). The CCD from the Li_r/LLZT sample is compared in Figure S6 (Supporting Information) to other $\text{Li}/\text{LLZO}/\text{Li}$ symmetric cells reported in the literature.^[8a,9,11b,24] Obviously, the CCD measured in the current work has the highest value for a garnet-type electrolyte, which implies that the present rub-coating technique provides excellent Li-ion transport property across the Li/LLZT interface.

To evaluate the long-term stability of the Li/LLZT interface and its ability to block lithium dendrite growth, the symmetric $\text{Li}_r/\text{LLZT}/\text{Li}_r$ cell was subjected to galvanostatic cycling at various current densities. As shown in Figure 2c, the symmetric cell can be successfully cycled at a current density of $\pm 13.3 \text{ mA cm}^{-2}$ with a capacity of 0.4 mAh cm^{-2} at room temperature for 500 cycles and exhibits a stabilized voltage polarization of about 0.2 V. For each cycle (insets of Figure 2c), the overpotential increases in the positive half cycle, implying the Li dissolution; it decreases in the negative half cycle, implying the Li deposition. This phenomenon is typical for the Li/garnet interface.^[22] EIS analysis was conducted to assess the impedance changes before and after the cycling tests. Figure S7 (Supporting Information) depicts that after the cycling tests, the cell impedance still consists of two distinct arcs, similar to that before the tests, which confirms that no shorting takes place after the cycling test. Moreover, after cycling tests, the cell impedance decreases, which is related to the locally formed lithium on the Li/LLZT interface or within the LLZT pellets during the stripping–plating process and agrees with previous literature.^[1g,11a,20f,25] In Figure 2d and Figure S8 (Supporting Information), the long-term stability of the Li/LLZT interface is tested by cycling the symmetric $\text{Li}_r/\text{LLZT}/\text{Li}_r$ cell at $\pm 2.2 \text{ mA cm}^{-2}$ with a capacity of 0.88 mAh cm^{-2} and at $\pm 0.1 \text{ mA cm}^{-2}$ with a capacity of 0.06 mAh cm^{-2} for 80 and 950 h, respectively. No sign of short circuiting is observed during the whole cycling test, stressing the stable and durable Li_r/LLZT interface. By contrast, as shown in Figure S9 (Supporting Information), the potential of the $\text{Li}_s/\text{LLZT}/\text{Li}_s$ cell exhibits a noisy profile with large voltage polarization before shorting at 70 h, suggesting that poor contact in Figure 1e,f leads to uneven Li plating and stripping across the Li_s/LLZT interface.^[15a] It is notable that from Figure 2b–d, the total resistances based on the Ohm's law are smaller than those estimated from the EIS results in Figure 1a and Figure S3a (Supporting Information). Similar phenomenon has been reported in other works.^[24g,26] The exact reason is unclear at this moment. Nevertheless, we speculate that under high current densities,

fast ion migration might be achieved as a result of the concerted migration of multiple lithium ions with low energy barriers, rather than isolated ion hopping.^[27] Also, the total resistances among the samples in Figure 2b–d are slightly different because we used different LLZT pellets in these electrochemical tests to make sure that we had fresh Li/SSE interfaces for each test. Thus, the pellet property may vary a little and this is common in pellet preparation by solid-state reaction.

2.2. Characterization of Li Metal–LLZT Interface

To understand the origin of the outstanding Li_r/LLZT interface performance, we employed time-of-flight secondary-ion mass spectrometry (TOF-SIMS) to perform an in-depth chemical analysis on the Li metals and the Li/LLZT interfaces. The surface of Li metal stored in glove box was investigated by TOF-SIMS depth profiling. Figure 3a,b shows that a layer of Li_2O exists on the Li surface. Here, the Li^- secondary ion (SI) signal represents Li from both Li_2O and metal Li, while O^{2-} represents the Li_2O . A false-color, 3D view of the sputtered volume during the depth profile in Figure 3b shows slight Li_2O penetration into the Li substrate, implying a rough Li surface. High-resolution chemical maps of two main species of interest, Li^- and O^{2-} , after 100, 1500, and 3500 s sputtering of the Li surface are presented in Figure S10 (Supporting Information). These maps confirm the coverage of Li_2O on the Li surface, which further implies that for $\text{Li}_s/\text{LLZO}/\text{Li}_s$ cells, the Li_s/LLZT interfaces are in fact separated by a layer of Li_2O .

The TOF-SIMS results of the Li_r/LLZT interface are shown in Figure 3c,d. A few interesting points can be extracted from these results. First, the focused ion beam secondary electron (FIB SE) image confirms a sharp and intimate interface between the Li metal and the LLZT ceramic. Second, the element depth analysis and the chemical maps of O and C after shallow (100 s) and heavy (4500 s) sputtering show the existence of O on the Li side at the beginning stage of sputtering; and as the sputtering proceeds, the O signal gets weaker. This means that after heavy sputtering, a true Li/LLZT interface can be obtained, at which Li covers fully and penetrates slightly into the LLZT surface. We believe that it is the direct contact between the fresh Li and the LLZT that leads to the above excellent electrochemical performance.

2.3. Effect of Li_2CO_3 on Garnet Surface

The effects of surface Li_2CO_3 of LLZT pellets on the Li/LLZT interface properties are specifically studied because it is widely accepted that the thin layer of Li_2CO_3 formed on the surface of lithium–garnets during sample handling or storage deteriorates the Li/garnet interface properties,^[4c,11c,16a,b,28] and tremendous efforts have been dedicated to suppressing, if not eliminating, the Li_2CO_3 formation.^{[4c,11]c,[16a,b,17]} Here, the LLZT pellets with surface layer of Li_2CO_3 were obtained by intentionally storing LLZT pellets in humid air for one week and the Li_2CO_3 layer was confirmed by the XRD (Figure S2, Supporting Information). As can be deduced from Figure S11 (Supporting Information), the thickness of Li_2CO_3 is around

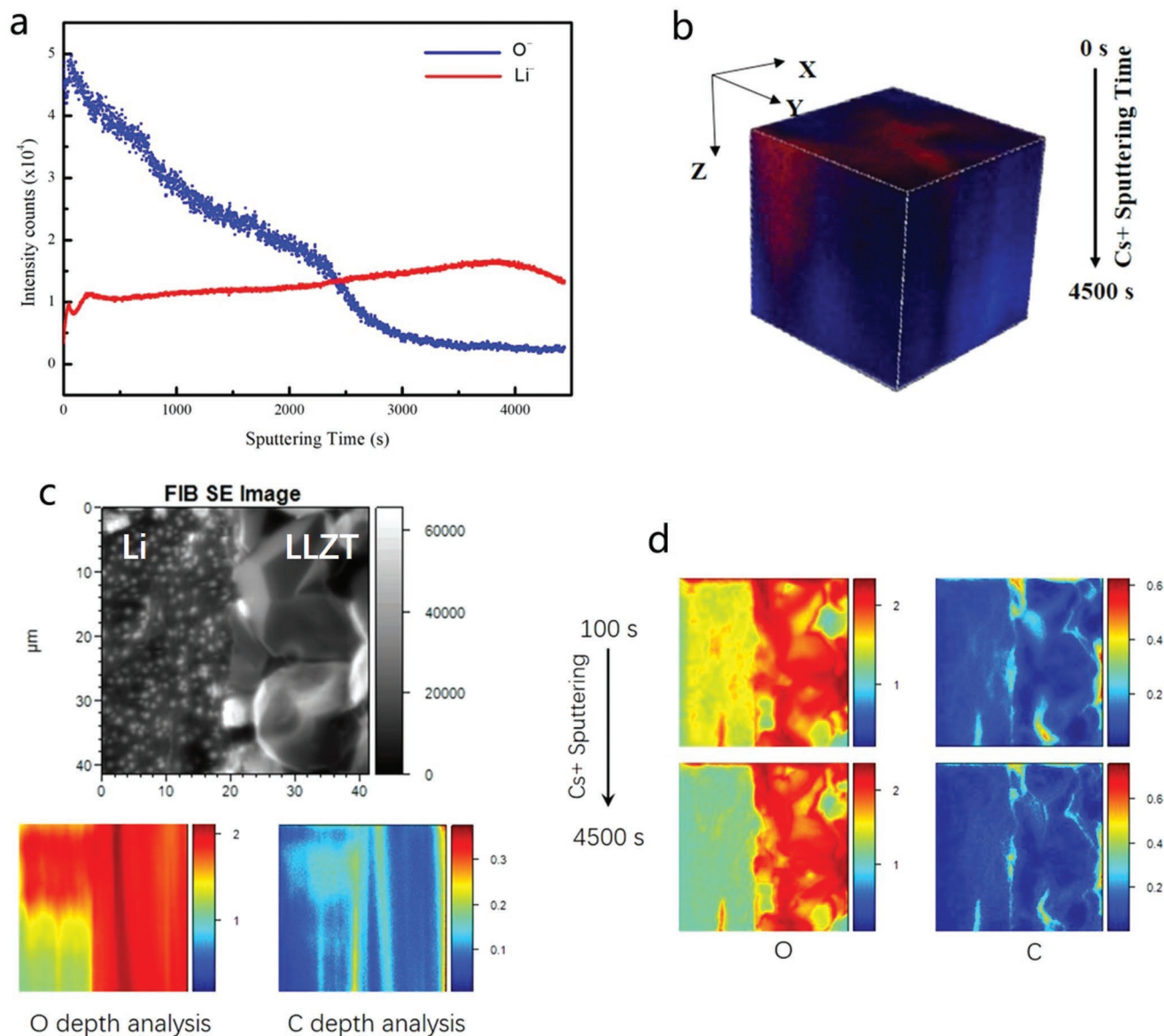


Figure 3. TOF-SIMS characterization of Li metal and the Li_t/LLZT interfaces. a) TOF-SIMS depth profiling of Li metal. b) A 3D view of the sputtered volume corresponding to the depth profile in (a) showing slight Li_2O penetration into the Li substrate. Red color represents oxygen and blue color represents lithium. c) TOF-SIMS depth profiling of the Li_t/LLZT interface. d) High-resolution maps ($40 \times 40 \mu\text{m}^2$) of the O and C secondary ion (SI) signals after shallow (100 s) and heavy (4500 s) sputtering.

3 μm . The symmetric cells were then assembled by rub coating molten Li metal. The EIS results (Figure 4a) of the symmetric cells show that the interfacial ASR is $492.6 \Omega \text{ cm}^2$, which is indeed substantially larger than that of the Li_t/LLZT interfaces ($6.95 \Omega \text{ cm}^2$) in Figure 1a. Nevertheless, as shown in Figure 4b, the symmetric cells are steadily cycled at 0.1 mA cm^{-2} for 50 h without shorting. The voltage profile is relatively stable and smooth, very different from those noisy and spiky voltage profiles previously reported for the garnet pellets with Li_2CO_3 surface layer.^[10b,17,18] The cell polarization voltage is about 0.022 V, in contrast to 0.015 V for the LLZT without Li_2CO_3 , and continuously increases with cycling, but no sign of shorting is observed. This suggests that LLZT

pellets, even with a surface Li_2CO_3 layer, render robust and stable Li/LLZT interface. The inset photograph in Figure 4a shows clearly that the Li_2CO_3 -coated LLZT pellets wet Li rather well. In fact, Figure S12 (Supporting Information) shows that pure Li_2CO_3 pellets can somewhat wet molten Li as well.

To investigate the Li/LLZT (with Li_2CO_3) interface in more details, we used TOF-SIMS to carry out elemental analysis. As shown in Figure 4c,d, there is clearly a layer of Li_2CO_3 on the LLZT surface, consistent with the XRD and Raman results above; moreover, SEM image shows that the Li metal bonds the Li_2CO_3 relatively tightly (Figure S13, Supporting Information). Thus, the surface Li_2CO_3 layer on LLZT pellets does not play a dominant role in determining the Li/LLZT interface performance.

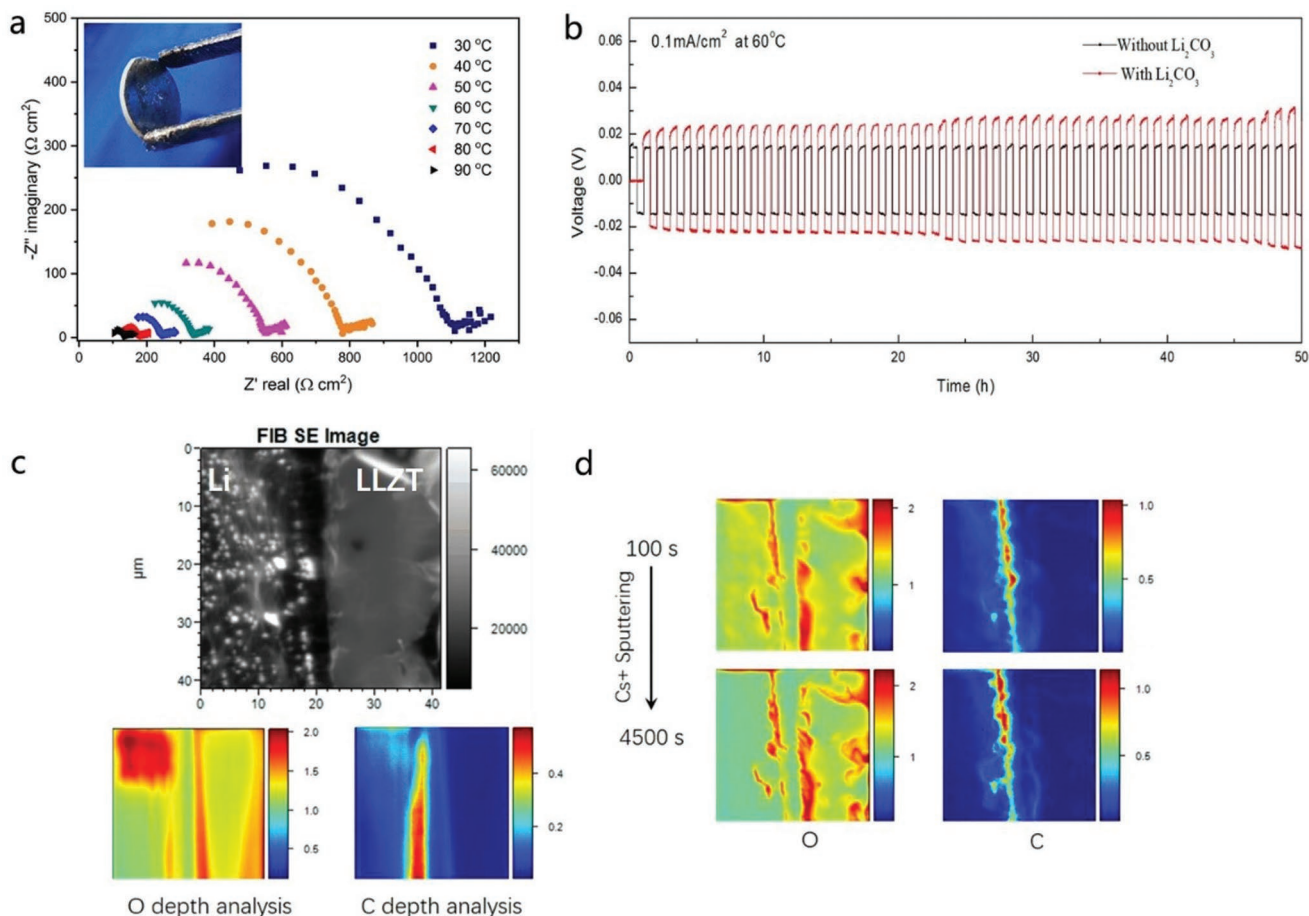


Figure 4. Characterization of the Li/LLZT (with Li_2CO_3) interfaces. a) Nyquist plots of Li_r/LLZT (with Li_2CO_3)/ Li_r symmetric cells at temperatures from 30 to 90 °C. Inset shows the melted Li metal on the LLZT surface with a Li_2CO_3 top layer. b) Galvanostatic cycling of Li_r/LLZT (with and without Li_2CO_3)/ Li_r at 0.1 mA cm^{-2} at 60 °C for 50 h. c) TOF-SIMS depth profiling of the Li_r/LLZT (with Li_2CO_3) interface. d) High-resolution maps ($40 \times 40 \mu\text{m}^2$) of the O and C SI signals after shallow (100 s) and heavy (4500 s) sputtering.

2.4. Computation of Li Metal and Garnet Interface

To further understand the wettability of Li metal on different surfaces, we conducted first-principle calculation to compare the interface formation energies of $\text{Li}_7\text{La}_3\text{Zr}_2\text{O}_{12}/\text{Li}$, $\text{Li}_{6.4}\text{La}_3\text{Zr}_{1.4}\text{Ta}_{0.6}\text{O}_{12}/\text{Li}$, $\text{Li}_2\text{CO}_3/\text{Li}$, and $\text{Li}_2\text{O}/\text{Li}$ systems. As shown in Figure 5 and Table S1 (Supporting Information), the interface formation energies of LLZO/Li, LLZT/Li, $\text{Li}_2\text{CO}_3/\text{Li}$, and $\text{Li}_2\text{O}/\text{Li}$ are -2.52 , -6.14 , -0.63 , and 0.23 J m^{-2} , respectively, which means the order of wettability with Li is $\text{LLZT} > \text{LLZO} > \text{Li}_2\text{CO}_3 > \text{Li}_2\text{O}$. Specifically, the formation energy of LLZO/Li is -2.52 J m^{-2} , suggesting the intrinsic lithiophilicity between lithium-garnets and Li metal, which is consistent with previous calculation results.^[11a] Moreover, the formation energy of LLZT/Li interfaces as low as -6.14 J m^{-2} implies that Ta doping can improve the wettability between Li-garnets and Li. Indeed, as shown in Figure S14 (Supporting Information), the interfacial ASR of Li/LLZO determined by EIS is $27.52 \Omega \text{ cm}^2$, which is higher than that of the Li_r/LLZT interfaces ($6.95 \Omega \text{ cm}^2$). The introduction of Li_2CO_3 will hinder lithium-garnets from wetting Li since the formation energy of $\text{Li}_2\text{CO}_3/\text{Li}$ interfaces

is merely -0.63 J m^{-2} . By contrast, the formation energy of $\text{Li}_2\text{O}/\text{Li}$ interfaces is 0.23 J m^{-2} , stressing that Li_2O does not wet well with Li metal. This implies that the Li_2O on the surface of Li might play a more important role in causing lithiophobicity than the Li_2CO_3 on the garnet surface.

2.5. Lithiophilicity Model for Garnet

The schematic in Figure 5e can describe the above experimental and computational results. The Li metal foil is intrinsically coated with a thin layer of Li_2O , when such Li metal foil is mechanically stacked onto lithium-garnets, poor Li/LLZT interface contact is obtained (Figures 1c and 5e) due to the high interface formation energies (Figure 5d). Many reported works have used a reactive interlayer (Al_2O_3 , Si, Au, C) to modify the garnet surface and decrease the Li/LLZO interfacial impedance,^[8a,10] which can be considered as using the interlayer to break the surface Li_2O layer on the lithium metal and obtain reaction wetting.^[29] By contrast, when the effect of this thin layer of Li_2O is eliminated by rubbing the LLZT pellets on molten Li and the fresh Li meets the LLZT surface, the intrinsic

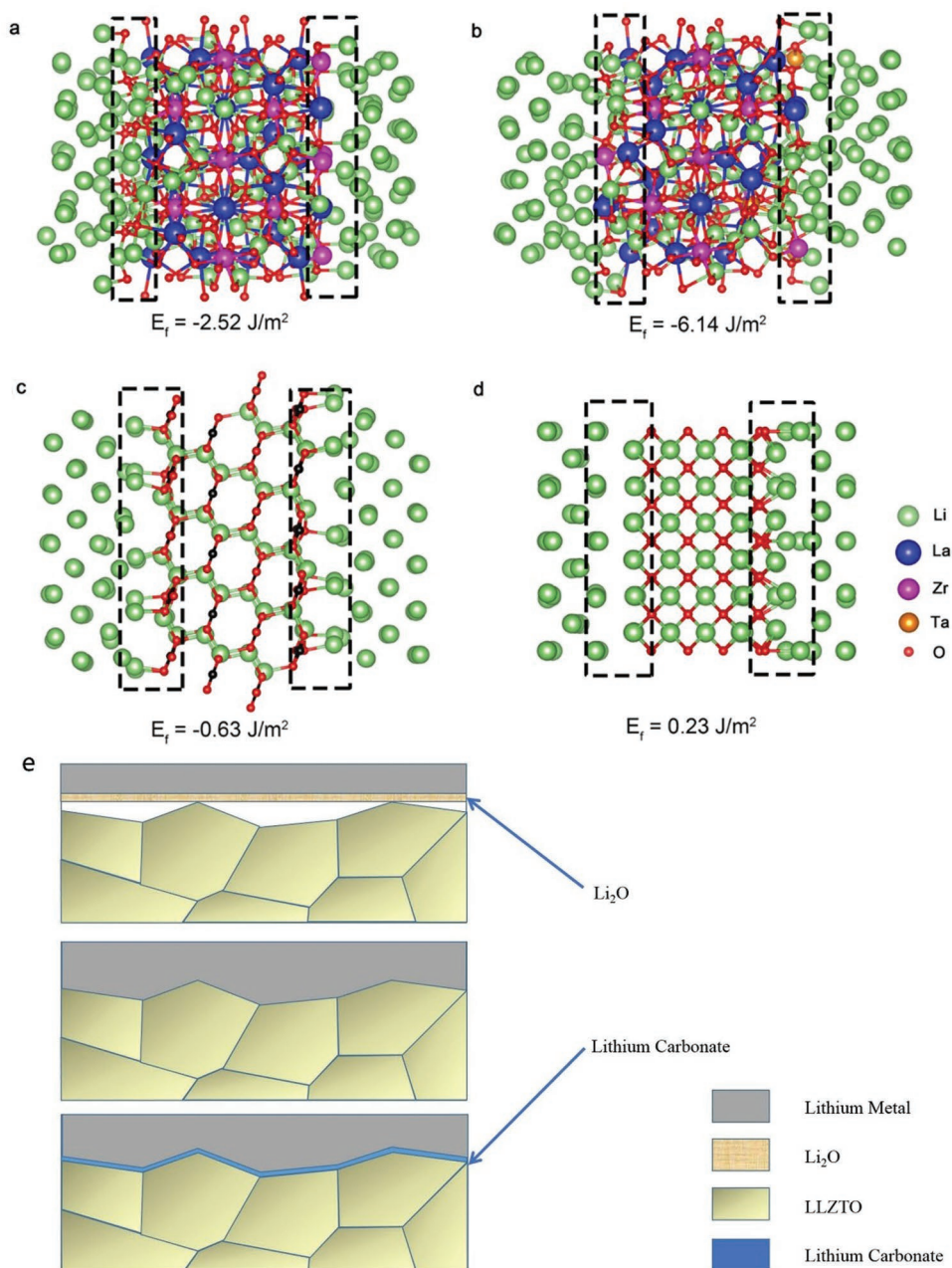


Figure 5. First-principle calculations of different interfaces. a–d) The optimized interface structures of LLZT/Li (a), LLZT/Li (b), $\text{Li}_2\text{CO}_3/\text{Li}$ (c), and $\text{Li}_2\text{O}/\text{Li}$ (d) and the corresponding interface formation energies. e) Schematic of different wetting behaviors of garnet surfaces with molten Li.

lithiophilicity of garnet exhibits and an intimate Li–LLZT contact with small interfacial impedance is realized (Figures 1d and 5e), providing a much higher CCD than these works using the interlayer. This Li/LLZT interface enables a room-temperature CCD as high as 13.3 mA cm^{-2} (Figure 2b), which implies excellent high-rate lithium cycling without dendrite formation. Even with an intentionally added thin layer of Li_2CO_3 on the garnet surface, the garnet pellets still show Li wetting property (Figures 4 and 5e). Moreover, about the relative density of the Li–garnets, on one hand, our previous results show that a relative density of 94% could not give us high CCD;^[15a,28,30] on the

other hand, the highly densified pellets (with relative density of 99%) only exhibit a current density of 0.5 mA cm^{-2} either.^[9] This implies that the previous studies paid much attention to the superficial impurity layer, the reactive interlayer, and the relative density of the Li–garnets, and neglected the crucial effect of the surface Li_2O layer on the lithium metal, which might in fact play an equally, if not more, important role in providing good Li/garnet interfaces.

Regarding the correlation between the CCD and the dendrite formation mechanism for solid electrolyte, an electronic conduction–induced dendrite formation mechanism

proposed earlier this year suggests that at elevated temperatures (i.e., 60 and 100 °C), the increased electronic conductivity of the garnet will cause Li ions to combine with electrons, hence reducing mobile Li ions and forming lithium dendrites within the garnet, for example, at the grain boundary.^[13] This is consistent with a recent computational study.^[31] These works further imply that lowering the electronic conductivity, rather than further increasing the ionic conductivity of solid electrolyte is critical to obtain a desirable Li/SSE interface, which appears to be demonstrated in a recent experimental work where by coating a thin electronically insulating buffer layer LiAlO₂ at the grain boundary, the CCD was increased from 0.4 to 0.75 mA cm⁻². It is true that in some particular circumstances, the excess electrons within the garnet may reduce Li⁺, but a more important question should be: what is the maximum CCD that a garnet-type electrolyte can provide with an intrinsic Li/garnet interface? Our work shows that the Li/LLZT interface can render a CCD of 13.3 mA cm⁻² at room temperature.

Using the current model, when the Li foil with the Li₂O surface layer is mechanically stacked on the garnet pellets, which is a common practice in most previous studies, small part of garnet will penetrate through the thin Li₂O film and directly contact the underneath fresh Li metal, thanks to the microscopically rough garnet surface. These direct yet sparse point contacts will function as charge centers as the charges accumulate during the Li plating, resulting in locally concentrated and increased current densities. The locally increased current densities lead to preferential Li deposition near the contacts and amplify the growth of Li dendrites. For other areas, the thin Li₂O film on the Li foil will prevent Li from wetting the garnet (Figure 5d). The existence of the surficial Li₂O film has been reported to hinder the wetting of molten lithium on metal substrates.^[32] By contrast, after exposing fresh Li surface, an area contact rather than a point contact can be obtained due to the intrinsic lithiophilicity of garnet (Figure 5e), which will significantly decrease the local current densities and subsequently inhibit Li-dendrite formation. Interestingly, in recent work by Hitz et al.,^[24g] molten lithium was infused into a Al₂O₃-coated porous garnet framework to form the lithium metal anode and a CCD of 10 mA cm⁻² was obtained. Part of the reason, as explained in that paper, is due to the fact that the pores of the porous garnet provide ≈40× higher surface area compared to a planar cell, leading to a true normalized current density at the interface of ≈0.25 mA cm⁻². Another important reason, based on our present work, is that during lithium impregnation, fresh lithium is exposed and directly contacts the garnet framework. Also remarkably, for the dense center garnet layer, the current density is still 10 mA cm⁻² no matter how much surface area gained from the porous framework, which confirms that garnet-type electrolyte, if engineered properly, can stand a current density of 10 mA cm⁻².

3. Conclusions

In summary, we effectively decrease the Li/garnet interfacial impedance and demonstrate the intrinsic lithiophilicity of garnet by eliminating the effect of the surface oxide layer on the lithium metal and making sure that lithium–garnets contact

fresh Li surfaces. The Li/garnet interfacial impedance was determined to be 6.95 Ω cm² at room temperature. It enables a critical current density as high as 13.3 mA cm⁻² at room temperature and stable high-rate lithium cycling of the symmetric cells for hundreds of cycles. The reasons for the excellent Li/garnet interface properties is analyzed through experiments and computations: 1) the superficial impurity layer, mainly Li₂O, on the Li metal leads to poor Li/garnet contact; 2) the thin Li₂CO₃ layer on garnet surface increases the Li/garnet interfacial impedance, yet plays a minor role in determining the Li/LLZT interface performance than the impurity layer on the Li metal; 3) the LLZT exhibits intrinsic lithiophilicity with an interface formation energy of -6.14 J m⁻². This work highlights that properly processing lithium metal anode is crucial for obtaining robust Li/electrolyte interfaces, which might impact the manufacturing process of future high energy density solid-state lithium batteries and other solid-state battery systems.

Supporting Information

Supporting Information is available from the Wiley Online Library or from the author.

Acknowledgements

This work was financially supported by the Natural Science Foundation of China (Grant Nos. 11304198 and 51972211), the National Key R&D Program of China (Grant No. 2017YFB0701900), the SJTU Materials Genome Initiative Center (Grant No. 15X190030002), and the SMC-Chen Xing Young Scholar Award of SJTU. Instrumental Analysis Center of SJTU and National Engineering Research Center for Nanotechnology are gratefully acknowledged for assisting with relevant experimental analysis. Center for High Performance Computing of SJTU is gratefully acknowledged for providing computational facilities for all the simulations.

Conflict of Interest

The authors declare no conflict of interest.

Keywords

critical current density, interface, lithium–garnet, solid electrolyte, solid-state lithium batteries

Received: July 30, 2019

Revised: November 12, 2019

Published online: December 6, 2019

- [1] a) B. Dunn, H. Kamath, J.-M. Tarascon, *Science* **2011**, *334*, 928; b) B. Nykvist, M. Nilsson, *Nat. Clim. Change* **2015**, *5*, 329; c) C.-X. Zu, H. Li, *Energy Environ. Sci.* **2011**, *4*, 2614; d) M. Armand, J. M. Tarascon, *Nature* **2008**, *451*, 652; e) J. W. Choi, D. Aurbach, *Nat. Rev. Mater.* **2016**, *1*, 16013; f) J. Liu, Z. Bao, Y. Cui, E. J. Dufek, J. B. Goodenough, P. Khalifah, Q. Li, B. Y. Liaw, P. Liu, A. Manthiram, Y. S. Meng, V. R. Subramanian, M. F. Toney, V. V. Viswanathan, M. S. Whittingham, J. Xiao, W. Xu, J. Yang, X.-Q. Yang, J.-G. Zhang, *Nat. Energy* **2019**, *4*, 180; g) T. Famprikis,

- P. Canepa, J. A. Dawson, M. S. Islam, C. Masquelier, *Nat. Mater.* **2019**, *18*, 1278; h) Z. Gao, H. Sun, L. Fu, F. Ye, Y. Zhang, W. Luo, Y. Huang, *Adv. Mater.* **2018**, *30*, 1705702; i) J. Wandt, C. Marino, H. A. Gasteiger, P. Jakes, R.-A. Eichel, J. Granwehr, *Energy Environ. Sci.* **2015**, *8*, 1358.
- [2] a) E. C. Everts, *Nature* **2015**, *526*, S93; b) M. Balaish, A. Kraysberg, Y. Ein-Eli, *Phys. Chem. Chem. Phys.* **2014**, *16*, 2801; c) M. Barghamadi, A. Kapoor, C. Wen, *J. Electrochem. Soc.* **2013**, *160*, A1256; d) K. Takada, *Acta Mater.* **2013**, *61*, 759; e) X. Hao, J. Zhu, X. Jiang, H. Wu, J. Qiao, W. Sun, Z. Wang, K. Sun, *Nano Lett.* **2016**, *16*, 2981; f) W. Na, A. S. Lee, J. H. Lee, S. S. Hwang, E. Kim, S. M. Hong, C. M. Koo, *ACS Appl. Mater. Interfaces* **2016**, *8*, 12852; g) C. Yang, K. Fu, Y. Zhang, E. Hitz, L. Hu, *Adv. Mater.* **2017**, *29*, 1701169.
- [3] a) R. Murugan, V. Thangadurai, W. Weppner, *Angew. Chem., Int. Ed.* **2007**, *46*, 7778; b) V. Thangadurai, S. Narayanan, D. Pinzaru, *Chem. Soc. Rev.* **2014**, *43*, 4714.
- [4] a) S. Ramakumar, C. Deviannapoorani, L. Dhivya, L. S. Shankar, R. Murugan, *Prog. Mater. Sci.* **2017**, *88*, 325; b) Q. Liu, Z. Geng, C. Han, Y. Fu, S. Li, Y.-b. He, F. Kang, B. Li, *J. Power Sources* **2018**, *389*, 120; c) H. Huo, Y. Chen, N. Zhao, X. Lin, J. Luo, X. Yang, Y. Liu, X. Guo, X. Sun, *Nano Energy* **2019**, *61*, 119; d) S. Zugmann, M. Fleischmann, M. Amereller, R. M. Gschwind, H. D. Wiemhöfer, H. J. Gores, *Electrochim. Acta* **2011**, *56*, 3926.
- [5] J. Yue, M. Yan, Y.-X. Yin, Y.-G. Guo, *Adv. Funct. Mater.* **2018**, *28*, 1707533.
- [6] N. J. Taylor, S. Stangeland-Molo, C. G. Haslam, A. Sharafi, T. Thompson, M. Wang, R. Garcia-Mendez, J. Sakamoto, *J. Power Sources* **2018**, *396*, 314.
- [7] a) S. Wang, H. Xu, W. Li, A. Dolocan, A. Manthiram, *J. Am. Chem. Soc.* **2018**, *140*, 250; b) C. Wang, Y. Gong, J. Dai, L. Zhang, H. Xie, G. Pastel, B. Liu, E. Wachsman, H. Wang, L. Hu, *J. Am. Chem. Soc.* **2017**, *139*, 14257.
- [8] a) C.-L. Tsai, V. Roddatis, C. V. Chandran, Q. Ma, S. Uhlenbruck, M. Bram, P. Heitjans, O. Guillon, *ACS Appl. Mater. Interfaces* **2016**, *8*, 10617; b) A. Sharafi, H. M. Meyer, J. Nanda, J. Wolfenstine, J. Sakamoto, *J. Power Sources* **2016**, *302*, 135.
- [9] Y. Suzuki, K. Kami, K. Watanabe, A. Watanabe, N. Saito, T. Ohnishi, K. Takada, R. Sudo, N. Imanishi, *Solid State Ionics* **2015**, *278*, 172.
- [10] a) X. Han, Y. Gong, K. Fu, X. He, G. T. Hitz, J. Dai, A. Pearse, B. Liu, H. Wang, G. Rubloff, Y. Mo, V. Thangadurai, E. D. Wachsman, L. Hu, *Nat. Mater.* **2017**, *16*, 572; b) B. Wu, S. Wang, J. Lochala, D. Desrochers, B. Liu, W. Zhang, J. Yang, J. Xiao, *Energy Environ. Sci.* **2018**, *11*, 1803; c) S. Xu, D. W. McOwen, L. Zhang, G. T. Hitz, C. Wang, Z. Ma, C. Chen, W. Luo, J. Dai, Y. Kuang, E. M. Hitz, K. Fu, Y. Gong, E. D. Wachsman, L. Hu, *Energy Storage Mater.* **2018**, *15*, 458; d) Y. Li, X. Chen, A. Dolocan, Z. Cui, S. Xin, L. Xue, H. Xu, K. Park, J. B. Goodenough, *J. Am. Chem. Soc.* **2018**, *140*, 6448.
- [11] a) J.-F. Wu, B.-W. Pu, D. Wang, S.-Q. Shi, N. Zhao, X. Guo, X. Guo, *ACS Appl. Mater. Interfaces* **2019**, *11*, 898; b) A. Sharafi, E. Kazyak, A. L. Davis, S. Yu, T. Thompson, D. J. Siegel, N. P. Dasgupta, J. Sakamoto, *Chem. Mater.* **2017**, *29*, 7961; c) L. Cheng, W. Chen, M. Kunz, K. Persson, N. Tamura, G. Chen, M. Doeff, *ACS Appl. Mater. Interfaces* **2015**, *7*, 2073.
- [12] a) J. van den Broek, S. Afyon, J. L. M. Rupp, *Adv. Energy Mater.* **2016**, *6*, 1600736; b) C. Yang, L. Zhang, B. Liu, S. Xu, T. Hamann, D. McOwen, J. Dai, W. Luo, Y. Gong, E. D. Wachsman, L. Hu, *Proc. Natl. Acad. Sci. USA* **2018**, *115*, 3770.
- [13] F. Han, A. S. Westover, J. Yue, X. Fan, F. Wang, M. Chi, D. N. Leonard, N. J. Dudney, H. Wang, C. Wang, *Nat. Energy* **2019**, *4*, 187.
- [14] Y. Ren, Y. Shen, Y. Lin, C.-W. Nan, *Electrochem. Commun.* **2015**, *57*, 27.
- [15] a) B. Xu, W. Li, H. Duan, H. Wang, Y. Guo, H. Li, H. Liu, *J. Power Sources* **2017**, *354*, 68; b) Z. Zhang, L. Zhang, C. Yu, X. Yan, B. Xu, L.-m. Wang, *Electrochim. Acta* **2018**, *289*, 254.
- [16] a) H. Duan, H. Zheng, Y. Zhou, B. Xu, H. Liu, *Solid State Ionics* **2018**, *318*, 45; b) W. Xia, B. Xu, H. Duan, Y. Guo, H. Kang, H. Li, H. Liu, *ACS Appl. Mater. Interfaces* **2016**, *8*, 5335; c) L. Cheng, C. H. Wu, A. Jarry, W. Chen, Y. Ye, J. Zhu, R. Kostecki, K. Persson, J. Guo, M. Salmeron, G. Chen, M. Doeff, *ACS Appl. Mater. Interfaces* **2015**, *7*, 17649.
- [17] Y. Shao, H. Wang, Z. Gong, D. Wang, B. Zheng, J. Zhu, Y. Lu, Y.-S. Hu, X. Guo, H. Li, X. Huang, Y. Yang, C.-W. Nan, L. Chen, *ACS Energy Lett.* **2018**, *3*, 1212.
- [18] M. He, Z. Cui, C. Chen, Y. Li, X. Guo, *J. Mater. Chem. A* **2018**, *6*, 11463.
- [19] J. Awaka, A. Takashima, K. Kataoka, N. Kijima, Y. Idemoto, J. Akimoto, *Chem. Lett.* **2011**, *40*, 60.
- [20] a) H. Buschmann, J. Dölle, S. Berendts, A. Kuhn, P. Bottke, M. Wilkening, P. Heitjans, A. Senyshyn, H. Ehrenberg, A. Lotnyk, V. Duppel, L. Kienle, J. Janek, *Phys. Chem. Chem. Phys.* **2011**, *13*, 19378; b) L. Cheng, E. J. Crumlin, W. Chen, R. Qiao, H. Hou, S. Franz Lux, V. Zorba, R. Russo, R. Kostecki, Z. Liu, K. Persson, W. Yang, J. Cabana, T. Richardson, G. Chen, M. Doeff, *Phys. Chem. Chem. Phys.* **2014**, *16*, 18294; c) W. Luo, Y. Gong, Y. Zhu, K. K. Fu, J. Dai, S. D. Lacey, C. Wang, B. Liu, X. Han, Y. Mo, E. D. Wachsman, L. Hu, *J. Am. Chem. Soc.* **2016**, *138*, 12258; d) K. Fu, Y. Gong, Z. Fu, H. Xie, Y. Yao, B. Liu, M. Carter, E. Wachsman, L. Hu, *Angew. Chem., Int. Ed.* **2017**, *56*, 14942; e) T. Liu, Y. Ren, Y. Shen, S.-X. Zhao, Y. Lin, C.-W. Nan, *J. Power Sources* **2016**, *324*, 349; f) C. Wang, Y. Gong, B. Liu, K. Fu, Y. Yao, E. Hitz, Y. Li, J. Dai, S. Xu, W. Luo, E. D. Wachsman, L. Hu, *Nano Lett.* **2017**, *17*, 565.
- [21] E. J. Cheng, A. Sharafi, J. Sakamoto, *Electrochim. Acta* **2017**, *223*, 85.
- [22] H. Koshikawa, S. Matsuda, K. Kamiya, M. Miyayama, Y. Kubo, K. Uosaki, K. Hashimoto, S. Nakanishi, *J. Power Sources* **2018**, *376*, 147.
- [23] T. Krauskopf, H. Hartmann, W. G. Zeier, J. Janek, *ACS Appl. Mater. Interfaces* **2019**, *11*, 14463.
- [24] a) J. Fu, P. Yu, N. Zhang, G. Ren, S. Zheng, W. Huang, X. Long, H. Li, X. Liu, *Energy Environ. Sci.* **2019**, *12*, 1404; b) Y. Song, L. Yang, W. Zhao, Z. Wang, Y. Zhao, Z. Wang, Q. Zhao, H. Liu, F. Pan, *Adv. Energy Mater.* **2019**, *9*, 1900671; c) A. Sharafi, C. G. Haslam, R. D. Kerns, J. Wolfenstine, J. Sakamoto, *J. Mater. Chem. A* **2017**, *5*, 21491; d) Y. Lu, X. Huang, Y. Ruan, Q. Wang, R. Kun, J. Yang, Z. Wen, *J. Mater. Chem. A* **2018**, *6*, 18853; e) J. Duan, W. Wu, A. M. Nolan, T. Wang, J. Wen, C. Hu, Y. Mo, W. Luo, Y. Huang, *Adv. Mater.* **2019**, *31*, 1807243; f) R. H. Basappa, T. Ito, H. Yamada, *J. Electrochem. Soc.* **2017**, *164*, A666; g) G. T. Hitz, D. W. McOwen, L. Zhang, Z. Ma, Z. Fu, Y. Wen, Y. Gong, J. Dai, T. R. Hamann, L. Hu, E. D. Wachsman, *Mater. Today* **2019**, *22*, 50.
- [25] L. E. Marbella, S. Zekoll, J. Kasemchainan, S. P. Emge, P. G. Bruce, C. P. Grey, *Chem. Mater.* **2019**, *31*, 2762.
- [26] C. Yang, H. Xie, W. Ping, K. Fu, B. Liu, J. Rao, J. Dai, C. Wang, G. Pastel, L. Hu, *Adv. Mater.* **2019**, *31*, 1804815.
- [27] X. He, Y. Zhu, Y. Mo, *Nat. Commun.* **2017**, *8*, 15893.
- [28] B. Xu, H. Duan, W. Xia, Y. Guo, H. Kang, H. Li, H. Liu, *J. Power Sources* **2016**, *302*, 291.
- [29] N. Eustathopoulos, R. Voytovych, *J. Mater. Sci.* **2016**, *51*, 425.
- [30] Y. Li, B. Xu, H. Xu, H. Duan, X. Lü, S. Xin, W. Zhou, L. Xue, G. Fu, A. Manthiram, J. B. Goodenough, *Angew. Chem., Int. Ed.* **2017**, *56*, 753.
- [31] H.-K. Tian, B. Xu, Y. Qi, *J. Power Sources* **2018**, *392*, 79.
- [32] J. Wang, H. Wang, J. Xie, A. Yang, A. Pei, C.-L. Wu, F. Shi, Y. Liu, D. Lin, Y. Gong, Y. Cui, *Energy Storage Mater.* **2018**, *14*, 345.